

Level density and γ -ray strength function in the odd-odd ^{238}Np nucleus

T. G. Tornyi,^{1,2,*} M. Guttormsen,¹ T. K. Eriksen,¹ A. Görgen,¹ F. Giacoppo,¹ T. W. Hagen,¹ A. Krasznahorkay,²
A. C. Larsen,¹ T. Renström,¹ S. J. Rose,¹ S. Siem,¹ and G. M. Tveten¹

¹*Department of Physics, University of Oslo, N-0316 Oslo, Norway*

²*Institute of Nuclear Research of the Hungarian Academy of Sciences (MTA Atomki), Debrecen, Hungary*

(Received 24 February 2014; published 28 April 2014)

The level density and γ -ray strength function in the quasicontinuum of ^{238}Np have been measured using the Oslo method. The level-density function follows closely the constant-temperature level-density formula and reaches 43×10^6 levels per MeV at $S_n = 5.488$ MeV of excitation energy. The γ -ray strength function displays a two-humped resonance at low-energy as also seen in previous investigations of Th, Pa, and U isotopes. The structure is interpreted as the scissors resonance and has an average centroid of $\omega_{\text{SR}} = 2.26(5)$ MeV and a total strength of $B_{\text{SR}} = 10.8(12)\mu_N^2$, which is in excellent agreement with sum-rule estimates. The scissors resonance is shown to have an impact on the $^{237}\text{Np}(n,\gamma)^{238}\text{Np}$ cross section.

DOI: [10.1103/PhysRevC.89.044323](https://doi.org/10.1103/PhysRevC.89.044323)

PACS number(s): 23.20.-g, 24.30.Gd, 27.90.+b

I. INTRODUCTION

Atomic nuclei in the actinide region are believed to be synthesized in explosive stellar environments purely by the rapid neutron-capture process. Therefore, to predict their abundances found on Earth [1,2], one has to know the various reaction rates for all isotopes including the ones with extreme neutron excess. Reaction rates are also vital for the modeling of future and existing nuclear reactors [3,4]. It is particularly important to ensure a reliable extrapolation in cases where measured data are insufficient or lacking.

The ^{237}Np isotope with a half-life of 2.14×10^6 years is one of the main constituents in nuclear spent fuel. In the former high-level waste repository in the Yucca Mountain, Nevada, USA about 40 tons of ^{237}Np are stored [5], and it is of great interest to find methods for transmuting this type of radioactive waste. In order to obtain high transmutation efficiency, the neutron fission-to-capture ratio should be determined for the particular isotope as function of neutron energy. Hence, accurate fission and capture cross sections are necessary to make reliable predictions [6].

The nuclear level density and γ -ray strength function (γSF) are important inputs in statistical Hauser-Feshbach reaction-rate calculations. These functions describe the average properties of excited nuclei in the quasicontinuum region, where the number of levels is too high to study individual states and their transitions. Here, the Oslo method [7,8] has been shown to be an excellent tool to determine simultaneously the level density and the γ -ray strength function (γSF).

Recently, the Oslo method was applied to the $^{231-233}\text{Th}$, $^{232,233}\text{Pa}$, and $^{237-239}\text{U}$ isotopes [9–11]. The level densities of all eight actinides follow closely the constant-temperature level-density formula. Furthermore, a large scissors resonance (SR) was observed in the γSF with a γ -energy centroid at $\omega_{\text{SR}} \approx 2.4$ MeV. This extra γ strength enhances the decay with γ rays relative to other decay branches such as particle emission or fission.

One would expect that the SR is present throughout the region of well-deformed actinides. The n_TOF collaboration [12] has recently reported on (n,γ) experiments on the ^{234}U , ^{237}Np , and ^{240}Pu isotopes. They verify a low-energy structure in ^{235}U and ^{241}Pu , but not in ^{238}Np , a result that is rather surprising. The odd-odd ^{238}Np nucleus has the same gross properties as other actinides, and the Oslo group has confirmed that the structure also appears in the odd-odd ^{232}Pa nucleus [11]. Thus, the n_TOF results on ^{238}Np have triggered us to investigate this case further.

The main purpose of the present work is to search for the SR in ^{238}Np and to determine the total level density and γSF . Furthermore, we present (n,γ) cross section from Hauser-Feshbach calculations using the measured level density and γSF as inputs. The calculations are compared with known (n,γ) data from literature.

The manuscript is organized as follows. Section II describes briefly the experimental methods, and in Sec. III the extraction and normalization of the level density and γSF are discussed. In Sec. IV the SR is presented, and extracted resonance parameters are compared to previous results and sum-rules estimates. In Sec. V the measured level density and γSF are used as inputs to Hauser-Feshbach calculations in order to estimate (n,γ) cross sections. Conclusions are drawn in Sec. VI.

II. EXPERIMENT

The experiment was performed with the MC-35 Scanditronix cyclotron at the Oslo Cyclotron Laboratory (OCL). The ^{237}Np target (thickness 0.200 mg/cm^2 and enrichment 99%), which had a carbon backing (thickness 0.020 mg/cm^2), was bombarded with a 13.5 MeV deuteron beam. Particle- γ coincidences were measured with the SiRi particle telescope and the CACTUS γ -detector system [13,14].

The 64 SiRi telescopes were placed in backward direction covering eight angles from $\theta = 126^\circ$ to 140° relative to the beam axis. This configuration was chosen to reduce the intense elastically scattered deuterons and to obtain a broad and rather high spin distribution that matches better to the spin

*tornyiom@gmail.com

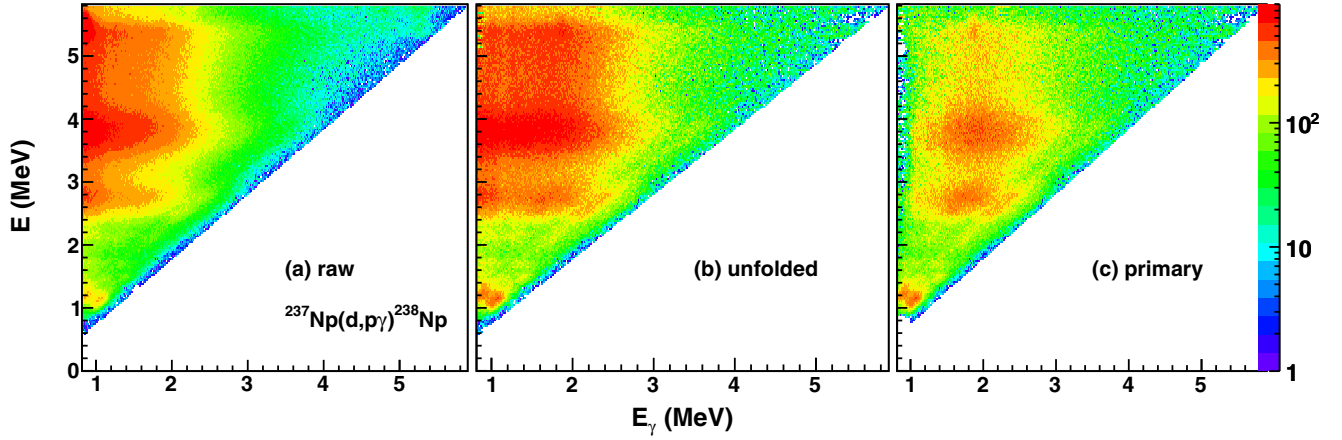


FIG. 1. (Color online) Initial excitation energy E versus γ -ray energy E_γ from particle- γ coincidences recorded with the $^{237}\text{Np}(d,p\gamma)^{238}\text{Np}$ reaction. The raw γ -ray spectra (a) are first unfolded by the NaI response function (b) and finally the primary or first-generation γ -ray spectra (c) are extracted as function of excitation energy E . The excitation and γ energy axis have dispersions of 14.0 keV/ch and 30.4 keV/ch, respectively.

distribution of available states in the quasicontinuum. The front and back detectors have thicknesses of 130 μm and 1550 μm , respectively. The CACTUS array consists of 28 collimated 5 in. \times 5 in. NaI(Tl) detectors with a total efficiency of 15.2% at $E_\gamma = 1.33$ MeV.

The E back detectors were used as master gates and the start for the time-to-digital-converter (TDC). One or more of the NaI detectors were used as individual TDC stops. In this way, prompt particle- γ coincidences with background subtraction could be sorted event by event. The proton events were selected by setting proper two-dimensional gates on the 64 ΔE - E matrices. From the kinematics of the reaction, the proton energies deposited in the telescopes were translated into initial excitation energy E in the residual ^{238}Np nucleus.

Figure 1 shows the first main steps of the Oslo method. After sorting the data into a raw matrix of initial excitation energy versus the NaI energy signal, Fig. 1(a), the matrix is unfolded [15] using the NaI response function for each excitation bin, Fig. 1(b). In Fig. 1(c) the first-generation (primary) γ -ray matrix $P(E, E_\gamma)$ is shown. Here, an iterative subtraction technique was applied to separate out the distribution of the first-generation γ s from the total γ cascade [16]. The technique is based on the assumption that the γ distribution is the same whether the levels were populated directly by the nuclear reaction or by γ decay from higher-lying states. This assumption is necessarily fulfilled when states have the same relative probability to be populated by the two processes, since γ -branching ratios are properties of the levels themselves.

The first-generation matrix P is built from the total matrix $P_{\text{gen}>0}$ of Fig. 1(b), where all γ s of all cascades are included. The matrix with higher generations $P_{\text{gen}>1}$ is obtained by weighting and summing the spectra at lower excitation energy. In principle, the first-generation matrix $P_{\text{gen}=1}$ is identical to the proper weighting function and obtained by an iterative procedure described in detail in Ref. [16].

The number of counts in the second- or higher-generation spectra $A_{\text{gen}>1}$ has to relate to the counts of the total spectrum $A_{\text{gen}>0}$. Since the γ multiplicity of the first-generation spectra

equals unity, we find

$$A_{\text{gen}>1} = \frac{M_\gamma(E) - 1}{M_\gamma(E)} A_{\text{gen}>0}. \quad (1)$$

Provided, that we have a correct normalization of the counts in the $P_{\text{gen}>1}$ matrix, the primary matrix is given by $P = P_{\text{gen}>0} - P_{\text{gen}>1}$. The average γ multiplicity from initial excitation energy E is given by

$$M_\gamma(E) = \frac{E}{\langle E_\gamma(E) \rangle}, \quad (2)$$

where $\langle E_\gamma(E) \rangle$ is the centroid of the total γ spectrum [Fig. 1(b)] at E .

Figure 2 shows the γ multiplicity for $E_\gamma > 0.45$ MeV as a function of initial excitation energy E . At the lower

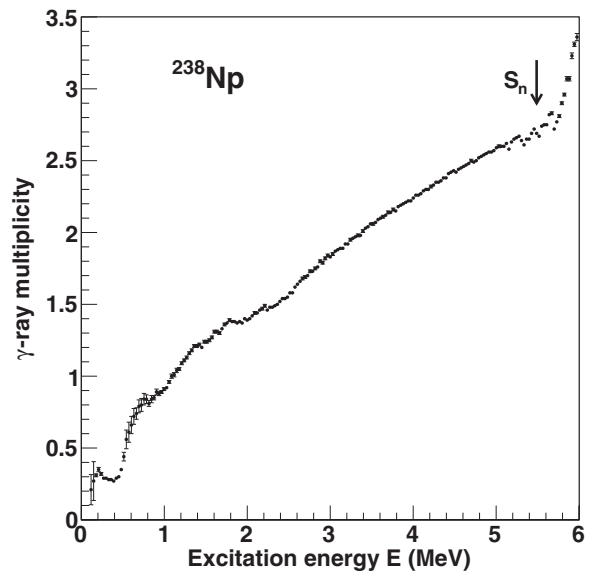


FIG. 2. γ -ray multiplicity for $E_\gamma > 0.45$ MeV as function of excitation energy E in ^{238}Np .

TABLE I. Parameters used to extract level density and γ SF (see text).

S_n (MeV)	a (MeV ⁻¹)	E_1 (MeV)	$\sigma(S_n)$	D_0 (eV)	$\rho(S_n)$ (10 ⁶ MeV ⁻¹)	$\rho(S_n)_{\text{red}}$ (10 ⁶ MeV ⁻¹)	$\langle\Gamma_\gamma(S_n)\rangle$ (MeV)
5.488	25.96	-0.84	8.28	0.57(3)	43.0(78)	22	40.8(12)

excitation energies, the multiplicity is seen to fluctuate since the decay routes become increasingly dependent on available levels of certain spin/parity and structure when approaching the ground state. Above $E = 2\text{--}3$ MeV, the decay seems to reveal a statistical behavior. To proceed with the Oslo method, we use only the region $E = 3.0\text{--}5.7$ MeV of the first-generation matrix of Fig. 1(c).

According to the Brink hypothesis [17], the γ -ray transmission coefficient \mathcal{T} is approximately independent of excitation energy. Thus, the first-generation matrix $P(E, E_\gamma)$ may be factorized as follows:

$$P(E, E_\gamma) \propto \mathcal{T}(E_\gamma) \rho(E - E_\gamma), \quad (3)$$

where $\rho(E - E_\gamma)$ is the level density at the excitation energy after the first γ ray has been emitted in the cascades. This factorization allows the disentanglement of the level density and γ -ray transmission coefficient. Note that no initial assumptions are made regarding the functional form of \mathcal{T} and ρ . However, the least-square fit of $\mathcal{T}\rho$ to the measured matrix P [see Eq. (3)] determines only the functional form of \mathcal{T} and ρ ; if one solution of the functions \mathcal{T} and ρ is known, one may construct infinitely many identical fits to the $P(E, E_\gamma)$ matrix by

$$\tilde{\rho}(E - E_\gamma) = A \exp[\alpha(E - E_\gamma)] \rho(E - E_\gamma), \quad (4)$$

$$\tilde{\mathcal{T}}(E_\gamma) = B \exp(\alpha E_\gamma) \mathcal{T}(E_\gamma). \quad (5)$$

The transformation parameters A , α , and B have then to be determined from other data, which is discussed in the next section.

III. NORMALIZATION

We need to find the A and α parameters of Eq. (4) in order to determine the level density. The two normalization points are determined at low excitation energy from the known level scheme [18] and at high energy from the density of neutron resonances following thermal (n, γ) capture at the neutron separation energy S_n . Here, the upper data point $\rho(S_n)$ is estimated from $\ell = 0$ neutron resonance spacings D_0 taken from RIPL-3 [19] assuming a spin distribution [20]

$$g(E = S_n, I) \simeq \frac{2I + 1}{2\sigma^2} \exp[-(I + 1/2)^2 / 2\sigma^2]. \quad (6)$$

The spin-cutoff parameter was determined from the global systematic study of level-density parameters by von Egidy and Bucurescu, who use a rigid-body moment of inertia approach [21]:

$$\sigma^2 = 0.0146A^{5/3} \frac{1 + \sqrt{1 + 4aU}}{2a}, \quad (7)$$

where A is the mass number, a is the level-density parameter, $U = E - E_1$ is the intrinsic excitation energy, and E_1 is the

back-shift parameter. Table I lists the D_0 , σ , and ρ values at S_n used to determine the level density. The a and E_1 parameters are taken from Ref. [21]. One should note that the spin distribution at such high excitation energies is not well known, and thus imposes a systematic uncertainty on our results.

Figure 3 demonstrates how the level density is normalized to the anchor points at low and high excitation energies. The level density follows closely the constant temperature formula with $\ln \rho \propto E/T_{\text{CT}}$ as also measured for other Th, Pa, and U isotopes [10]. It is interesting to see that only a small fraction of the levels, even at low excitation energies, have been observed in the odd-odd ^{238}Np . The reason is of course the very high-level density, e.g., at 1 MeV of excitation energy the average distance between levels is ≈ 1 keV, only.

The level density is closely related to the entropy of the system, from which thermodynamic quantities such as temperature and heat capacity can be extracted. This will not be further elaborated here since the properties of the level-density function observed for ^{238}Np are very similar to those observed for $^{237\text{--}239}\text{U}$ [10].

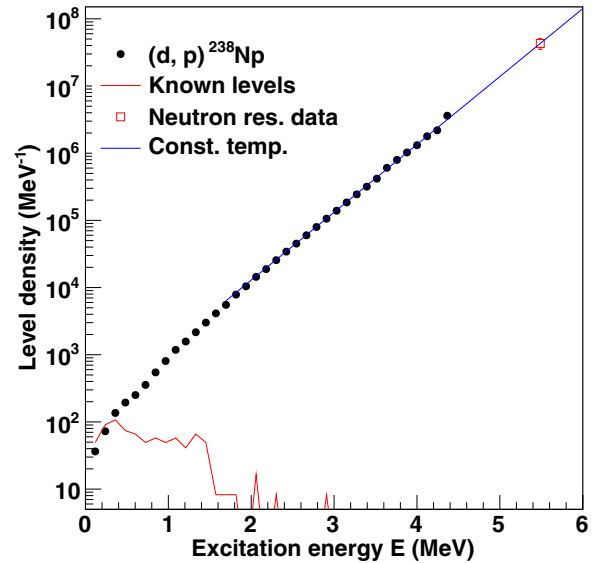


FIG. 3. (Color online) Level density for ^{238}Np . The experimental data are normalized to the level density of known discrete levels at low excitation energy E (red solid line) and the level density extracted from known neutron resonance spacings D_0 at the neutron separation energy S_n . The connection between $\rho(S_n)$ (the upper right data points) and our experimental data are made with a constant-temperature formula with $T_{\text{CT}} = 0.43$ MeV. The odd-odd ^{238}Np nucleus has an extreme high level density of ≈ 43 million levels per MeV at the neutron separation energy of $S_n = 5.488$ MeV.

The light-ion (d, p) reaction used in this work may not populate the highest spin levels available in the nucleus, which in turn could influence the shape of the observed primary γ spectra P . Since the transmission coefficient T is assumed to be independent of spin, the observed P matrix should be fitted with the product $T\rho_{\text{red}}$, where the reduced level density is extracted by assuming a lower value of ρ at S_n . Since there are uncertainties in the total $\rho(S_n)$ through the estimate of σ and also the actual spin distribution brought into the nuclear system by the specific reaction, the extracted slope of T becomes rather uncertain.

The parameter B controls the scaling of the transmission coefficient $T(E_\gamma)$. Here we use the average, total radiative width $\langle\Gamma_\gamma\rangle$ at S_n assuming that the γ decay is dominated by dipole transitions. For initial spin I and parity π , the width is given by [22]

$$\langle\Gamma_\gamma\rangle = \frac{1}{2\pi\rho(S_n, I, \pi)} \sum_{I_f} \int_0^{S_n} dE_\gamma B T(E_\gamma) \rho(S_n - E_\gamma, I_f), \quad (8)$$

where the summation and integration run over all final levels with spin I_f that are accessible by $E1$ or $M1$ transitions with energy E_γ .

Since our spin distribution for the reaction is likely to be lower than the spin distribution of the available levels, the standard normalization procedure of the Oslo method [7,23] to determine the α parameter for the transmission coefficient in Eq. (5) is not reliable. Instead we compare the γ SF with the extrapolation of known data from photo-nuclear reactions.

The γ SF for dipole radiation can be calculated from the transmission coefficient $T(E_\gamma)$ by [19]

$$f(E_\gamma) = \frac{1}{2\pi} \frac{T(E_\gamma)}{E_\gamma^3}. \quad (9)$$

These data are compared with the strength function derived from the cross section σ of photonuclear reactions by [19]

$$f(E_\gamma) = \frac{1}{3\pi^2\hbar^2c^2} \frac{\sigma(E_\gamma)}{E_\gamma}, \quad (10)$$

where the factor $1/3\pi^2\hbar^2c^2$ takes the value $8.6737 \times 10^{-8} \text{ mb}^{-1} \text{ MeV}^{-2}$. In Fig. 4 the γ SF derived from $^{237}\text{Np}(\gamma, x)$ cross section by Berman *et al.* [24] is shown (x means all possible ejectiles, as well as fission fragments). We assume that this strength does not vary much from ^{237}Np to ^{238}Np , as pointed out for the two $^{236,238}\text{U}$ isotopes [11].

Since our data cover γ energies below S_n , we have to extrapolate the (γ, x) data to lower energies. For the double-humped giant electric dipole resonance (GEDR) we fit the data with two enhanced generalized Lorentzians (EGLOs) as defined in RIPL [19], but with a constant temperature

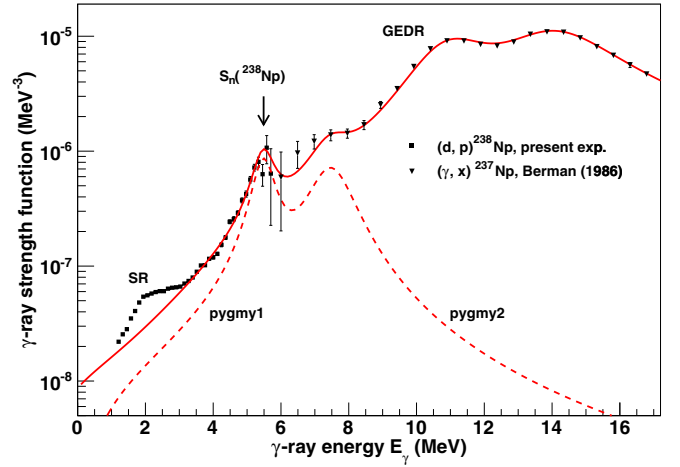


FIG. 4. (Color online) Experimental γ SF from the present (d, p) ^{238}Np experiment (black filled squares) compared with the estimated underlying γ SF (red curve), which represents the strength expected without the SR. The (γ, x) data (black filled triangles) are taken from Berman *et al.* [24].

parameter of the final states T_f , in accordance with the Brink hypothesis. In addition the (γ, x) data [24] reveal a knee at around 7.5 MeV indicating a resonancelike structure (labeled pygmy2 in Fig. 4). We also note the steep flank of our γ SF data from 4–5 MeV of γ energy. In order to match this increase in the γ SF another pygmy is postulated at around 5.5 MeV. The two pygmy resonances are described by simple Lorentzians:

$$f_{\text{pyg}} = \frac{1}{3\pi^2\hbar^2c^2} \frac{\sigma_{\text{pyg}} \Gamma_{\text{pyg}}^2 E_\gamma}{(E_\gamma^2 - \omega_{\text{pyg}}^2)^2 + \Gamma_{\text{pyg}}^2 E_\gamma^2}. \quad (11)$$

The sum of the two GEDR and the two pygmy γ SFs are shown as a solid red curve in Fig. 4. The four sets of resonance parameters are listed in Table II.

We have also tested another approach of modeling the γ SF in the 4–8 MeV region. One broad Gaussian shape at 6.5 MeV gives approximately the same fit to the available data. However, we feel that there are no arguments to adopt a Gaussian shape for a resonance structure. Since the choice of one broad Lorentzian fails to reproduce the data, we keep to the assumption of two narrow pygmies as shown in Fig. 4.

Provided that the extrapolation in Fig. 4 (red solid curve) is reliable, we may assume that this γ SF represents the baseline with no additional strength from other resonances. Thus, we normalize the measured γ SF to this underlying background. Here, the α parameter is adjusted to obtain the right slope of the observed γ SF; the level density at S_n had to be reduced from 43×10^6 to 22×10^6 levels per MeV because of the lack of high spin levels due to the low angular momentum transfer

TABLE II. Resonance parameters used for the γ SF extrapolation.

$\omega_{E1,1}$ (MeV)	$\sigma_{E1,1}$ (mb)	$\Gamma_{E1,1}$ (MeV)	$\omega_{E1,2}$ (MeV)	$\sigma_{E1,2}$ (mb)	$\Gamma_{E1,2}$ (MeV)	T_f (MeV)	ω_{pyg1} (MeV)	σ_{pyg1} (mb)	Γ_{pyg1} (MeV)	ω_{pyg2} (MeV)	σ_{pyg2} (mb)	Γ_{pyg2} (MeV)
11.3	970	3.0	14.6	1520	4.4	0.2	5.5	50	0.7	7.5	60	1.4

TABLE III. Scissors resonance parameters of ^{238}Np and its sum-rule estimates [Eqs. (15) and (16), see text].

Deformation	Lower resonance				Upper resonance				Total	Sum rule		
δ	$\omega_{\text{SR},1}$ (MeV)	$\sigma_{\text{SR},1}$ (mb)	$\Gamma_{\text{SR},1}$ (MeV)	$B_{\text{SR},1}$ (μ_N^2)	$\omega_{\text{SR},2}$ (MeV)	$\sigma_{\text{SR},2}$ (mb)	$\Gamma_{\text{SR},2}$ (MeV)	$B_{\text{SR},2}$ (μ_N^2)	ω_{SR} (MeV)	B_{SR} (μ_N^2)	ω_{SR} (MeV)	B_{SR} (μ_N^2)
0.25	1.95(4)	0.41(4)	0.61(5)	4.5(6)	2.48(6)	0.49(6)	0.90(10)	6.3(10)	2.26(5)	10.8(12)	2.2	9.9

of the (d, p) reaction. The B parameter was determined by use of Eq. (8) in order to reproduce the experimental γ width $\langle \Gamma_\gamma \rangle$ listed in Table I.

IV. SCISSORS RESONANCE

Figure 5 shows the γSF where the assumed Lorentzian shape line of Fig. 4 has been subtracted. The observed structure, which is interpreted as the SR, is in accordance with previous observations in the $^{231-233}\text{Th}$, $^{232,233}\text{Pa}$, and $^{237-239}\text{U}$ isotopes [9–11]. Thus, our finding is in strong disagreement with the $(n, \gamma)^{238}\text{Np}$ results of the n_TOF group that found no evidence for the SR structure [12].

The SR is split into two components where the strengths of each component is given by a set of resonance parameters:

$$B = \frac{9\hbar c}{32\pi^2} \left(\frac{\sigma \Gamma}{\omega} \right). \quad (12)$$

The resonance parameters of the lower and upper component, as well as the total strength and average energy centroid are listed in Table III.

We find that the separation in energy between the two components is much smaller than previously seen for Th, Pa, and U [11]; $\Delta\omega_{\text{SR}} = 0.89(15)$ compared to $0.53(6)$ MeV for ^{238}Np . In addition the higher-lying component takes the main strength contrary to the other actinides where the low-lying strength carried almost 2/3 of the strength. The total strength is the same as for the other actinides within the uncertainties.

Recent high-quality measurements at the High-Intensity γ -ray Source (HI γ S) at the Triangle Universities Nuclear Laboratory (TUNL) has discovered more strength than for previous (γ, γ') measurements in this mass region [25–27]. In ^{232}Th a strength of $B_{\text{SR}} = 4.3(6)\mu_N^2$ at $\omega_{\text{SR}} = 2.5(4)$ MeV has been reported [28] and for ^{238}U there has been measured $B_{\text{SR}} = 8(1)\mu_N^2$ at $\omega_{\text{SR}} = 2.6(6)$ MeV [29].

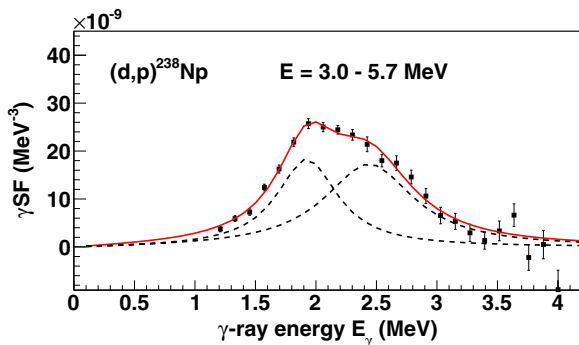


FIG. 5. (Color online) The extracted γSF for the scissors resonance in the quasi-continuum of ^{238}Np .

During the last decades several SR models have been proposed to explain the results of the (γ, γ') and (e, e') reactions [30]. Very recent theoretical work on the scissors mode by Balbutsev, Molodtsova, and Schuck [31] postulates a new additional mode, the isovector spin scissors mode, which may explain the apparent splitting of the scissors structure. However, the results of these calculations are rather qualitative at the present stage as pairing correlations are not taken into account. Furthermore, an important challenge is to explain why the splitting appears in the actinides and not in the rare-earth region.

In this work we have chosen the sum-rule approach [32], which is a rather fundamental way to predict both ω_{SR} and B_{SR} consistently. We follow the description of Enders *et al.* [33] with the exception that the ground-state moment of inertia will be replaced by the rigid-body moment of inertia. The outline for the quasicontinuum was recently presented [11], and we only give a summary of the formulas here.

The inversely and linearly energy-weighted sum rules are given by [11]

$$S_{+1} = \frac{3}{2\pi} \Theta_{\text{rigid}} \delta^2 \omega_D^2 \left(\frac{Z}{A} \right)^2 \xi [\mu_N^2 \text{MeV}], \quad (13)$$

$$S_{-1} = \frac{3}{16\pi} \Theta_{\text{rigid}} \left(\frac{2Z}{A} \right)^2 [\mu_N^2 \text{MeV}^{-1}]. \quad (14)$$

The two sum rules can now be utilized to extract the SR centroid and strength:

$$\omega_{\text{SR}} = \sqrt{S_{+1}/S_{-1}} = |\delta| \omega_D \sqrt{2\xi}, \quad (15)$$

$$\begin{aligned} B_{\text{SR}} &= \sqrt{S_{+1}S_{-1}} = \frac{3}{4\pi} \left(\frac{Z}{A} \right)^2 \Theta_{\text{rigid}} |\delta| \omega_D \sqrt{2\xi} \\ &= \frac{3}{4\pi} \left(\frac{Z}{A} \right)^2 \Theta_{\text{rigid}} \omega_{\text{SR}}. \end{aligned} \quad (16)$$

The rigid-body moment of inertia is taken as

$$\Theta_{\text{rigid}} = \frac{2}{5} m_N r_0^2 A^{5/3} (1 + 0.31\delta), \quad (17)$$

with $r_0 = 1.15$ fm and δ is the nuclear quadrupole deformation¹ taken from Ref. [34]. The reduction factor

$$\xi = \frac{\omega_Q^2}{\omega_Q^2 + 2\omega_D^2} \quad (18)$$

¹The quadrupole deformation parameter δ relates to lowest order to ϵ_2 and β_2 as $\delta \approx \epsilon_2 \approx \beta_2 \sqrt{45/16\pi}$.

depends on the IVGDR and ISGQR frequencies of

$$\omega_D \approx (31.2A^{-1/3} + 20.6A^{-1/6})(1 - 0.61\delta)\text{MeV}, \quad (19)$$

$$\omega_Q \approx 64.7A^{-1/3}(1 - 0.3\delta)\text{MeV}. \quad (20)$$

The location of the IVGDR from systematics [Eq. (19)] gives $\omega_D = 11.3$ MeV. However, the GEDR structures of Fig. 4 have clearly a higher average centroid. From the GEDR resonance parameters of Table II we find $\omega_D = 13.4$ MeV, which we adopt for the sum-rule estimates.

The two last columns of Table III show the predicted ω_{SR} and B_{SR} from the sum-rule estimates. Both values are in excellent agreement with our measurements.

V. CALCULATIONS OF THE (n, γ) CROSS SECTION

The γ SF in the quasicontinuum is the quantity that directly relates to the reaction rates in, e.g., astrophysical environments. For example for the r process, which involves nuclei with extreme N/Z ratios, the decrease in neutron-separation energy with neutron number is expected to give an increasing impact from the SR on the reaction rates. The SR represents also an

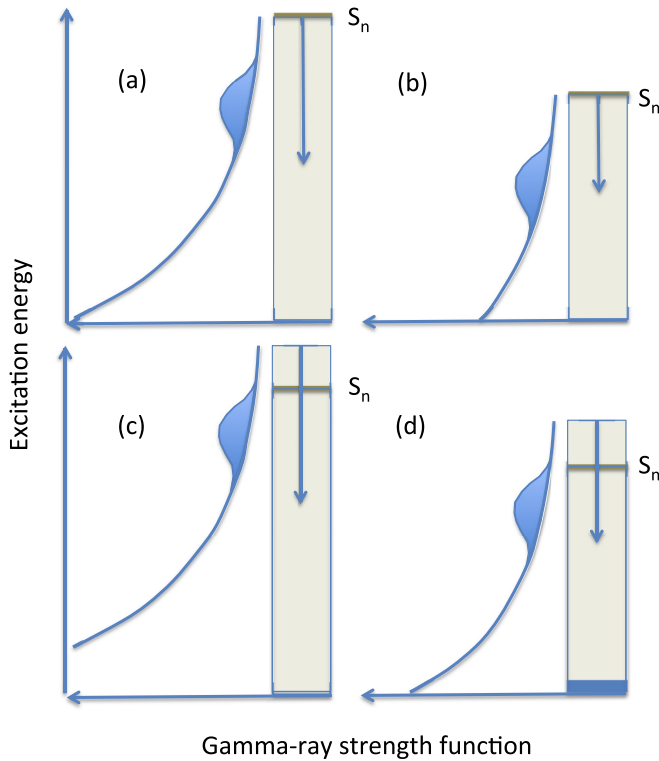


FIG. 6. (Color online) Schematic view of how the SR (blue bump) influences the γ -decay rates. The scenarios are: (a) $E \approx S_n$ and high S_n , (b) $E \approx S_n$ and low S_n , (c) $E > S_n$ and high S_n , and (d) $E > S_n$ and low S_n . If the centroid of the γ energies (arrow) overlaps with the centroid of the SR, the γ branch may increase significantly (up to a factor of two). The ^{238}Np nucleus with a relative high separation energy of $S_n = 5.488$ MeV, corresponds to case (a). With neutron energies of several MeV, the influence of the SR will diminish.

important ingredient for the simulations of fuel cycles for fast nuclear reactors.

In Fig. 6 the influence of the SR is schematically shown for four cases. It is obvious that if the initial state see much of the high-energy tail of the γ SF, the low-lying SR strength will have less importance. This happens in Figs. 6(a) and 6(c). The higher overlap of the SR with the first-generations γ s appears in Figs. 6(b) and 6(d). In ^{238}Np the binding energy is relatively high with $S_n = 5.488$ MeV [Fig. 6(a)], which means that only the high-energy part of the SR strength distribution comes into play.

In order to study the impact of the SR for ^{238}Np , we have performed calculations of the (n, γ) cross section with the TALYS code [35,36]. Experimental (n, γ) cross sections are rather well known for ^{238}Np , making this a good test ground for such calculations. In particular, a recent experiment at the DANCE facility [5] has provided data with small statistical errors for incoming neutron energies up to ≈ 300 keV.

For the TALYS input we have used functions that describe the observed level density and γ SF (data from Figs. 3 and 4, respectively). For the neutron optical-model potential, we have used the global parametrization of Koning and Delaroche [37], but with adjusted values for the parameter a_V using a scaling factor of 0.65 to obtain agreement with the evaluated s -wave neutron strength function of $S_0 = 1.02(6) \times 10^{-4}$ [38].

Figure 7 shows the results of the cross-section calculations. The TALYS output (blue curve) is in excellent agreement with the experimentally measured (n, γ) cross sections from Refs. [5,39]. The agreements for all neutron energies above the resonance region of $E_n \geq 300$ eV give confidence to the observed γ SF as well as the level density. The increase in cross section due to the SR reaches a maximum of $\approx 25\%$ for

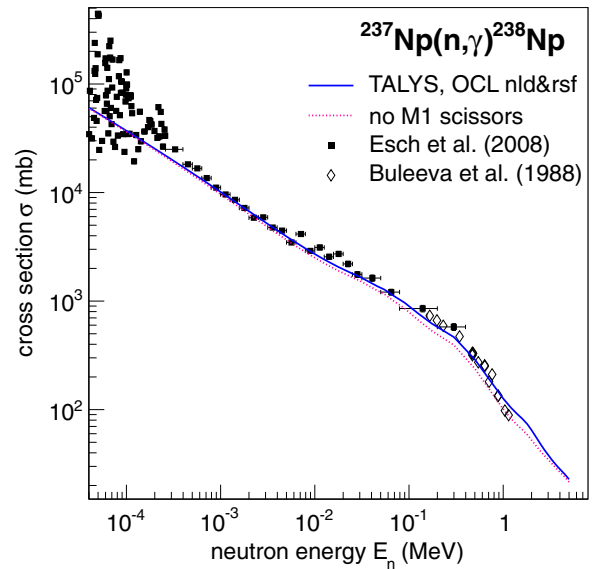


FIG. 7. (Color online) Calculated $^{237}\text{Np}(n, \gamma)^{238}\text{Np}$ cross section using level density and γ SF models in accordance with the data of this work. The predictions including the $M1$ scissors mode (blue curve) and without (dashed line) are compared with measured data from Esch *et al.* [5] (black squares) and Buleeva *et al.* [39] (open diamonds).

1-MeV incoming neutrons. The reason for the rather small influence of the $M1$ scissors resonance on the (n, γ) cross section for this case is discussed in connection with Fig. 6; the inclusion of the SR has less impact because the high-energy part of the γ SF dominates the γ -decay probability. For the highest neutron energies in Fig. 7 ($E_n \geq 5$ MeV), the SR has no practical impact on the cross section.

VI. CONCLUSIONS

The level density and γ SF of ^{238}Np have been determined using the Oslo method. The level density shows a constant-temperature behavior similar to other actinides as recently reported for $^{231-233}\text{Th}$, $^{232,233}\text{Pa}$ and $^{237-239}\text{U}$ [10,11].

We observe an excess in the γ SFs in the $E_\gamma = 1\text{--}4$ MeV region, which is interpreted as the SR in the quasicontinuum. These findings are in contradiction with the n_TOF results from the $(n, \gamma)^{238}\text{Np}$ reaction, but in agreement with expectations for the actinide region. The underlying strength of the SR has been subtracted by extrapolating the assumed strength

from the tails of other resonances; the double-humped GEDR and the two pygmy resonances. The SR shows a splitting into two components, however the two components are closer in energy than observed for the other actinides. The sum rule applied to the quasicontinuum assuming a rigid-body moment of inertia, describes very well the centroid and strength of the SR.

The observed level density and γ SF have been used as inputs in Hauser-Feshbach calculations with the TALYS code. The agreement with previously measured (n, γ) cross sections is very gratifying. The SR strength gives a maximum increase of 25% on the calculated cross section for 1-MeV neutrons.

ACKNOWLEDGMENTS

We would like to thank J. C. Müller, E. A. Olsen, A. Semchenkov, and J. Wikne at the Oslo Cyclotron Laboratory for providing the stable and high-quality deuterium beam during the experiment. This work was supported by the Research Council of Norway (NFR).

-
- [1] M. Arnould, S. Goriely, and K. Takahashi, *Phys. Rep.* **450**, 97 (2007).
 - [2] F. Käppeler *et al.*, *Rev. Mod. Phys.* **83**, 157 (2011).
 - [3] M. B. Chadwick *et al.*, *Nucl. Data Sheets* **112**, 2887 (2011).
 - [4] G. Aliberti, G. Palmiotti, M. Salvatores, T. K. Kim, T. A. Taiwo, M. Anitescu, I. Kodeli, E. Sartori, J. C. Bosq, and J. Tommasi, *Ann. Nucl. Energy* **33**, 700 (2006).
 - [5] E. I. Esch, R. Reifarth, E. M. Bond, T. A. Bredeweg, A. Couture, S. E. Glover, U. Greife, R. C. Haight, A. M. Hatarik, R. Hatarik, M. Jandel, T. Kawano, A. Mertz, J. M. O'Donnell, R. S. Rundberg, J. M. Schwantes, J. L. Ullmann, D. J. Vieira, J. B. Wilhelmy, and J. M. Wouters, *Phys. Rev. C* **77**, 034309 (2008).
 - [6] G. Aliberti, G. Palmiotti, M. Salvatores, and C. G. Stenberg, *Nucl. Sci. Eng.* **146**, 13 (2004).
 - [7] A. Schiller *et al.*, *Instrum. Methods Phys. Res. A* **447**, 498 (2000).
 - [8] A. C. Larsen *et al.*, *Phys. Rev. C* **83**, 034315 (2011).
 - [9] M. Guttormsen *et al.*, *Phys. Rev. Lett.* **109**, 162503 (2012).
 - [10] M. Guttormsen *et al.*, *Phys. Rev. C* **88**, 024307 (2013).
 - [11] M. Guttormsen *et al.*, *Phys. Rev. C* **89**, 014302 (2014).
 - [12] C. Guerrero *et al.*, *J. Korean Phys. Soc.* **59**, 1510 (2011).
 - [13] M. Guttormsen, A. Bürger, T. E. Hansen, and N. Lietaer, *Nucl. Instrum. Methods Phys. Res. A* **648**, 168 (2011).
 - [14] M. Guttormsen *et al.*, *Phys. Scr. T* **32**, 54 (1990).
 - [15] M. Guttormsen, T. S. Tveter, L. Bergholt, F. Ingebrechtsen, and J. Rekstad, *Nucl. Instrum. Methods Phys. Res. A* **374**, 371 (1996).
 - [16] M. Guttormsen, T. Ramsøy, and J. Rekstad, *Nucl. Instrum. Methods Phys. Res. A* **255**, 518 (1987).
 - [17] D. M. Brink, Ph.D. thesis, Oxford University, 1955 (unpublished).
 - [18] Data extracted using the NNDC On-Line Data Service from the ENSDF database.
 - [19] R. Capote *et al.*, Reference Input Library, RIPL-2 and RIPL-3, available online at <http://www-nds.iaea.org/RIPL-3/>
 - [20] A. Gilbert and A. G. W. Cameron, *Can. J. Phys.* **43**, 1446 (1965).
 - [21] T. von Egidy and D. Bucurescu, *Phys. Rev. C* **72**, 044311 (2005); **73**, 049901(E) (2006).
 - [22] J. Kopecky and M. Uhl, *Phys. Rev. C* **41**, 1941 (1990).
 - [23] A. Voinov, M. Guttormsen, E. Melby, J. Rekstad, A. Schiller, and S. Siem, *Phys. Rev. C* **63**, 044313 (2001).
 - [24] B. L. Berman, J. T. Caldwell, E. J. Dowdy, S. S. Dietrich, P. Meyer, and R. A. Alvarez, *Phys. Rev. C* **34**, 2201 (1986).
 - [25] R. D. Heil, H. H. Pitz, U. E. P. Berg, U. Kneissl, K. D. Hummel, G. Kilgus, D. Bohle, A. Richter, C. Wesselborg, and P. von Brentano, *Nucl. Phys. A* **476**, 39 (1988).
 - [26] J. Margraf, A. Degener, H. Friedrichs, R. D. Heil, A. Jung, U. Kneissl, S. Lindenstruth, H. H. Pitz, H. Schacht, U. Seemann, R. Stock, C. Wesselborg, P. von Brentano, and A. Zilges, *Phys. Rev. C* **42**, 771 (1990).
 - [27] O. Yevetska, J. Enders, M. Fritzsche, P. von Neumann-Cosel, S. Oberstedt, A. Richter, C. Romig, D. Savran, and K. Sonnabend, *Phys. Rev. C* **81**, 044309 (2010).
 - [28] A. S. Adekola, C. T. Angell, S. L. Hammond, A. Hill, C. R. Howell, H. J. Karwowski, J. H. Kelley, and E. Kwan, *Phys. Rev. C* **83**, 034615 (2011).
 - [29] S. L. Hammond, A. S. Adekola, C. T. Angell, H. J. Karwowski, E. Kwan, G. Rusev, A. P. Tonchev, W. Tornow, C. R. Howell, and J. H. Kelley, *Phys. Rev. C* **85**, 044302 (2012).
 - [30] K. Heyde, P. von Neumann-Cosel, and A. Richter, *Rev. Mod. Phys.* **82**, 2365 (2010), and references therein.
 - [31] E. B. Balbutsev, I. V. Molodtsova, and P. Schuck, *Phys. Rev. C* **88**, 014306 (2013).
 - [32] E. Lipparini and S. Stringari, *Phys. Rep.* **175**, 103 (1989).
 - [33] J. Enders, P. von Neumann-Cosel, C. Rangacharyulu, and A. Richter, *Phys. Rev. C* **71**, 014306 (2005).
 - [34] S. Goriely, N. Chamel, and J. M. Pearson, *Phys. Rev. Lett.* **102**, 152503 (2009).
 - [35] A. J. Koning, S. Hilaire, and M. C. Duijvestijn, TALYS-1.0, in *Proceedings of the International Conference on Nuclear Data for Science and Technology*, 2227 April 2007, Nice, France,

- edited by O. Bersillon, F. Gunsing, E. Bauge, R. Jacqmin, and S. Leray (EDP Sciences, Les Ulis, 2008), p. 211.
- [36] S. Goriely, S. Hilaire, and A. J. Koning, *Astron. Astrophys.* **487**, 767 (2008).
- [37] A. J. Koning and J. P. Delaroche, *Nucl. Phys. A* **713**, 231 (2003).
- [38] S. F. Mughabghab, *Atlas of Neutron Resonances*, 5th ed. (Elsevier Science, Amsterdam, 2006).
- [39] N. N. Buleeva, A. N. Davletshin, O. A. Tipunkov, S. V. Tikhonov, and V. A. Tolstikov, *Atomnaya Energiya* **65**, 348 (1988).